A Route to Nanoscopic Materials *via* Sequential Infiltration Synthesis on Block Copolymer Templates

Qing Peng,[†] Yu-Chih Tseng,[‡] Seth B. Darling,[‡,*] and Jeffrey W. Elam[†,*]

[†]Energy Systems Division and [‡]Center for Nanoscale Materials, Argonne National Laboratory, 9700 S. Cass Avenue, Argonne, Illinois 60439, United States

ABSTRACT Sequential infiltration synthesis (SIS), combining stepwise molecular assembly reactions with self-assembled block copolymer (BCP) substrates, provides a new strategy to pattern nanoscopic materials in a controllable way. The selective reaction of a metal precursor with one of the pristine BCP domains is the key step in the SIS process. Here we present a straightforward strategy to selectively modify self-assembled polystyrene-*block*-poly(methyl methacrylate) (PS-*b*-PMMA) BCP thin films to enable the SIS of a variety of materials including SiO_2, ZnO, and W. The selective and controlled interaction of trimethyl aluminum with carbonyl groups in the PMMA polymer domains generates Al-CH_3/Al—OH sites inside the BCP scaffold which can seed the subsequent growth of a diverse range of materials without requiring complex block copolymer design and synthesis.

KEYWORDS: atomic layer deposition · sequential infiltration · block copolymer · nano · silicon dioxide

Patterned nanomaterials with well-controlled morphology over macroscopic length scales have attracted substantial interest due to their potential applications in energy, sensors, biomedicine, and other technologies.[1−3] Block copolymers (BCPs), which can self-assemble into highly ordered arrays of nanostructures, have been recognized as a promising way to generate patterned nanofeatures.[3−6] The size, shape, and composition of ordered domains in BCPs can be tuned by changing the molecular weight and chemical composition.[3−6] To broaden the scope of materials—and hence functionalities—available to such structures, ordered domains provided by self-assembled BCP thin films have been used as nanoreactors or templates for confining/templating the growth of features of other materials.[3−15] To date, with BCPs as the scaffold, various gas phase and liquid phase processes have been utilized to synthesize patterned nanomaterials.[3−15] However, these methods are limited in terms of large scale controllability in the fabrication steps, complexity during the synthesis, and catalyst usage.[3−6]

Recently we introduced sequential infiltration synthesis (SIS) as a method to synthesize patterned nanofeatures with tunable dimensions by using a BCP of fixed domain size as the template.[16] SIS is related to atomic layer deposition (ALD), a cyclic, gas phase process for depositing thin films based on controlled surface reactions.[17−19] Because of the controlled stepwise reactions, SIS offers unprecedented precision in tuning the patterned feature size.[16] Atomic layer deposition has also previously been applied to block copolymer templates with the aim of generating nanomaterials; however, those systems relied on the inter-material boundary surface of the block copolymer templates to direct the materials growth.[20,21] In contrast, with the SIS method, controlled reactions between the infiltrated metal precursors and polymer chains in specific domains are used to direct the growth of the corresponding inorganic materials *within* the BCP nanodomains. In principle, SIS can be adapted to grow different materials by synthesizing customized block copolymers to effect a selective interaction with the appropriate metal precursor. However, the design and synthesis of new block copolymers can be complex, and altering the chemistry of the individual blocks can have dramatic and unanticipated effects on the self-assembly.

Here we present an alternative and more general strategy to selectively modify BCP domains for the SIS growth of a range of inorganic nanomaterials including SiO_2, ZnO, and W. The mechanism is shown schematically in Figure 1. It has been reported that long ALD exposure times allow gaseous reactants such as trimethyl aluminum (TMA) and H_2O to diffuse through soft matter and react with active sites within the material.[22−25] The key step here is to exploit this capability to selectively modify the poly(methyl methacrylate) (PMMA) domains in a polystyrene

* Address correspondence to jelam@anl.gov, darling@anl.gov.

Received for review January 25, 2011 and accepted May 5, 2011.

Published online May 05, 2011
10.1021/nn2003234

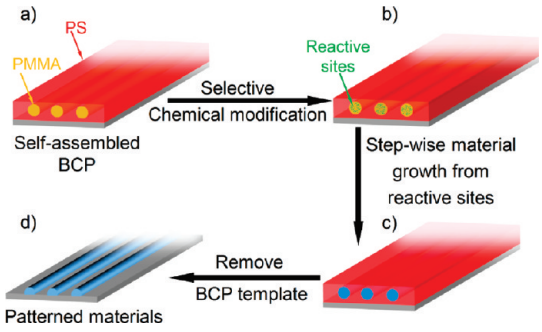

Figure 1. Simplified mechanism for the nanoscopic materials generation process with self-assembled BCPs as the template. Two key steps: (1) Chemically modifying the PMMA domains with the controlled reaction between trimethyl aluminum and the organic units in PMMA; (2) reaction sites generated from the chemical modification step promote selective growth of different materials by sequential infiltration synthesis. Material growth could also be affected by reactant diffusion.

(PS)-*b*-PMMA BCP through the stepwise controlled reaction between TMA and the carbonyl groups on the PMMA chains.[16] The $-Al-CH_3/-Al-OH$ groups formed inside the PMMA domains provide reactive sites for catalyzing or nucleating the subsequent SIS of other materials which otherwise would not grow within the PMMA. Through this method we can prepare patterned nanofeatures of a variety of materials without the need to synthesize specialized BCPs to accommodate the corresponding SIS chemistries. Since SIS adapts chemistries from ALD and Al_2O_3 ALD is well-studied,[18,26,27] the rich existing knowledge of nucleation and growth behavior of different materials *via* ALD on Al−OH surfaces provides general guidance for SIS using $-Al-CH_3/-Al-OH$ as nucleation sites. Moreover, as chemical modification of the PS-*b*-PMMA BCP template is performed after the assembly process, the self-assembly behavior of the BCP is not affected.

RESULTS AND DISCUSSION

The chemistry of an acid-catalyzed sol−gel reaction between $SiCl_4/Si(OC_2H_5)_4$ and H_2O has been widely used for fabricating patterned SiO_2 nanofeatures with BCP templates.[9,12] This localized synthesis process is difficult to control due to homogeneous reactions.[9,12] Recently, catalyzed ALD was demonstrated for well-controlled rapid SiO_2 growth,[28,29] and the reaction mechanism for this process has been determined.[28,29] The rapid SiO_2 growth is initiated from a TMA exposure. The resulting Al atoms in the $-Al-CH_3$ or $-Al-OH$ ligands then act as a catalyst for the subsequent insertion and polymerization reactions of silanol to form SiO_2. The SiO_2 growth in this process is controllable and the growth rate per cycle is dictated by the competition between silanol diffusion and the cross-linking reaction between siloxane chains.[28,29] On the basis of this mechanism, if one can selectively localize $Al-CH_3/Al-OH$ groups within one of the BCP domains, the subsequent silanol polymerization catalyzed by these groups should generate SiO_2 nanopatterns[28,29] so that acid/base catalysts such as HCl can be avoided. For instance, TMA can selectively coordinate to carbonyl groups inside the PMMA domains of the PS-*b*-PMMA BCP thin film,[16] and the resulting Al sites should then catalyze silanol polymerization and grow SiO_2 selectively in the PMMA domains.

Figure 2 panels a and b show FESEM images of the fingerprint pattern of SiO_2 nanocylinders synthesized using this method. The sample was prepared at 125 °C by first exposing the BCP substrate to TMA vapor for 400 s, purging with N_2 for 1200 s, exposing to silanol vapor for 400 s, again purging with N_2 for 1200 s, and finally heating at 400 °C for 12 h. The SiO_2 surface topography shown in Figure 2a,b retains the original order of the self-assembled block copolymer template (PS_{485}-*b*-$PMMA_{201}$). The width of the PS and PMMA domains of the BCP template is ~30 nm and the center-to-center space between domains is ~60 nm.[16] The higher resolution FESEM image in Figure 2b shows detailed features of the SiO_2 nanocylinders which have diameters of 37.1 ± 3.7 nm, that is, bigger than the original PMMA domain size in the PS-*b*-PMMA BCP template. However, the gaps between the domains can be clearly observed. This structure suggests that the SiO_2 growth initiated within the PMMA domains and then migrated into the PS domains once the dimensions exceeded those of the original PMMA cylinders. Moreover, by tuning the microdomain orientation of the BCP template, dense and ordered arrays of SiO_2 nanoposts could be synthesized as shown in Figures 2c,d. The diameter of the nanoposts is 35.4 ± 2.1 nm and is comparable to the diameter of the SiO_2 nanocylinders shown in Figure 2a,b. The clear separation between each SiO_2 nanocylinder indicates that the residual TMA inside of PS domains is negligible; otherwise a continuous SiO_2 film would be formed. On the basis of the mechanism of Al-catalyzed SiO_2 ALD,[28] one could further tune the SiO_2 nanofeature size by adjusting the reaction temperature, process pressure, and/or tri(tert-pentoxy) silanol (TPS) partial pressure during the SIS process. Although here the SIS reaction is carried within a complex three-dimensional polymer matrix, the general principles of the rapid catalytic SiO_2 growth mechanism still applies so that the SiO_2 growth should stop when all Al atoms are capped. This principle offers better controllability and large-scale uniformity than the ones relying on homogeneous reactions.[9,12] XPS analysis of the nanostructured silica sample showed only Si and O and some adventitious carbon while the Al concentration was below the XPS detection limit (Figure 3). These data provide evidence that the Al atoms are buried underneath the SiO_2, indicating that the Al-catalyzed reaction has terminated.

The $-Al-OH$ sites in the PMMA microdomains formed by treating PS-*b*-PMMA BCP with 1−2 cycles

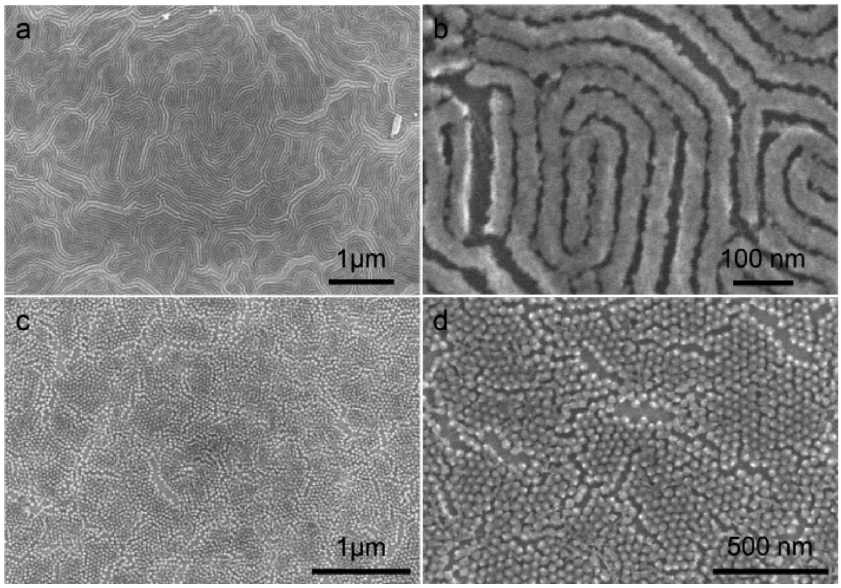

Figure 2. FESEM images of SiO_2 cylindrical pattern (a, b) and nanopost pattern (c, d) on Si wafer formed by 1 cycle catalytic SiO_2 SIS from TMA and silanol followed by O_2 plasma treatment.

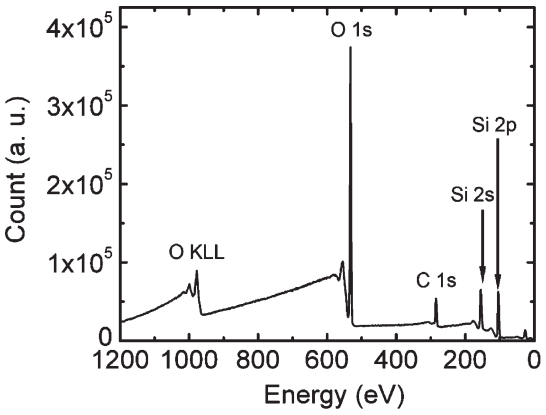

Figure 3. X-ray photoelectron spectrum of PS-*b*-PMMA block copolymer after treatment with one cycle SiO_2 SIS and thermal calcination. The atomic composition of Si, O, and C are 30%, 54%, and 16%, respectively. C is ascribed to adventitious contamination.

of Al_2O_3 by SIS can promote the growth of other materials (e.g., ZnO[30,31] and W[32]) which do not have direct selective chemistry with the pure PS-*b*-PMMA polymer. To explore this hypothesis, ZnO SIS with diethyl zinc and H_2O was performed on a PS-*b*-PMMA BCP film after 1 cycle Al_2O_3 SIS pretreatment.[16] As shown in Figure 4b, the ordered nanocylindrical pattern resulting from 1 Al_2O_3 SIS cycle (60/300/60/300 s) followed by 3 ZnO SIS cycles (300/300/300/300 s) at 85 °C is clear under FESEM. The width of the cylinders (19.4 ± 3.2 nm) is smaller than the domain size of the PMMA (~30 nm) and bigger than the Al_2O_3 cylinders resulting from 1 cycle Al_2O_3 SIS (Figure 4a). The corresponding AFM image and line scan for this sample are shown in Figure 4c,e. Control experiments were performed without the Al_2O_3 SIS seeding step using five cycles of ZnO SIS at 85 °C onto a pristine PS-*b*-PMMA BCP thin film. In contrast to the results discussed above, no features were observed under FESEM for this sample after removing the BCP template. The AFM image and corresponding line scan for this control sample are shown in Figures 4d,f which indicate a subtle pattern suggesting a weak preferential interaction between the DEZ and the PMMA domains compared with the PS domains. The different cylinder heights shown in Figure 4d–f and Figure 4c–e indicate that the –Al–OH sites in the PMMA microdomains substantially enhanced the selective growth of ZnO SIS in the PMMA domains compared with the PS domains. Since the ZnO features resemble the expected pattern from the PMMA domains, the data in Figure 4 indicate that the ZnO growth initiates at the –Al–OH groups within the PMMA domains through sequential infiltration and reaction from the DEZ and H_2O. Moreover, the smooth cylinder surface and comparatively smaller feature size relative to the original PMMA domains argue that the ZnO growth begins inside of the PMMA rather than at the interfacial boundary of the pristine BCP polymer as observed in previous reports.[20]

As an additional demonstration, we performed tungsten SIS at 85 °C onto PS-*b*-PMMA thin films with and without the Al_2O_3 SIS pretreatment. W SIS uses alternating exposures to Si_2H_6 and WF_6, and it would be challenging to synthesize BCPs with selective chemistry toward these precursors. Al–OH species are known to promote the nucleation of W ALD on polymers.[32] Consequently, treating PS-*b*-PMMA films using TMA should cause the SIS W to grow selectively within the PMMA domains. Figure 5a shows that organized nanostructures result from one Al_2O_3 SIS cycle followed by 10 W SIS cycles (60/300/60/300 s) and an O_2 plasma treatment. Compared with the

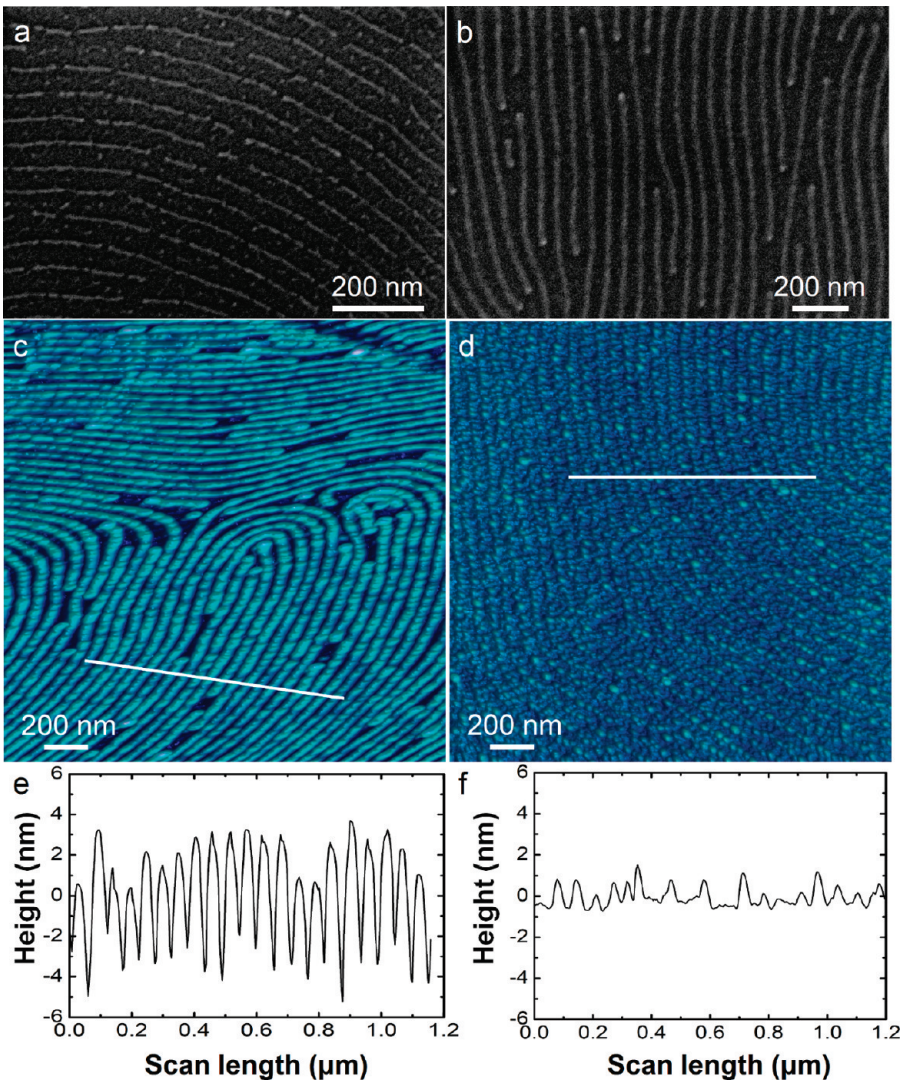

Figure 4. FESEM images of cylindrical patterns on Si wafer formed by (a) one cycle of Al_2O_3 SIS and (b) one cycle of Al_2O_3 SIS followed by three cycles of ZnO SIS. (c, e) AFM image and the line scan of sample from one cycle Al_2O_3 SIS followed by three cycles ZnO SIS. (d, f) AFM image and line scan of the pattern of sample from five cycles ZnO SIS on PS-*b*-PMMA thin film. For all samples, PS-*b*-PMMA BCP was removed by O_2 plasma.

nanofeatures resulting from a single SIS Al_2O_3 cycle (Figure 4a), the cylinder width is much larger (25.9 ± 1.9 nm) and broken regions are not observed. In contrast, a control sample prepared using only 10 W SIS cycles but no Al_2O_3 SIS pretreatment yielded no detectable features by FESEM (Supporting Information, Figure S1). These findings confirm that the W SIS is inhibited on the pure polymers,[24] and enhanced by Al−OH sites. Twenty W SIS cycles yielded wider cylinders (41.8 ± 2.7 nm) as illustrated by Figure 5b,d. The presence of W was confirmed by XRF (Figure 6). Figure 5b reveals that the cylinders have a smooth top surface but rougher, less continuous sidewalls suggesting preferential reaction on the surface of the PMMA domains compared with inside of the domains. This might result from the relatively slow diffusion of the bulky WF_6, particularly with increasing SIS cycles as the structure freezes hindering further diffusion within the polymer. This finding suggests that SIS might involve a complex interplay between diffusion and reaction for some materials, and a detailed investigation is underway to achieve a more complete understanding of these processes. Nevertheless, the clear gaps between the W lines provide evidence that the W growth originates in the PMMA domains and progresses as a stepwise heterogeneous reaction.

With the use of 2 cycles of Al_2O_3 SIS prior to the 20 cycles W SIS (Figure 5d), nanocylinder features with larger diameters (43.6 ± 3.1 nm) were formed due to the greater density of Al−OH reactive sites. Although the nanocylinders resulting from 20 cycles of W were larger than the PMMA domain size, the center-to-center spacing of these features, 55.7 ± 3.2 nm for 1 cycle Al_2O_3 pretreatment (Figure 5b) and 55.4 ± 3.0 nm and 2 cycles Al_2O_3 pretreatment (Figure 5d), is consistent with the corresponding periodicity in the original

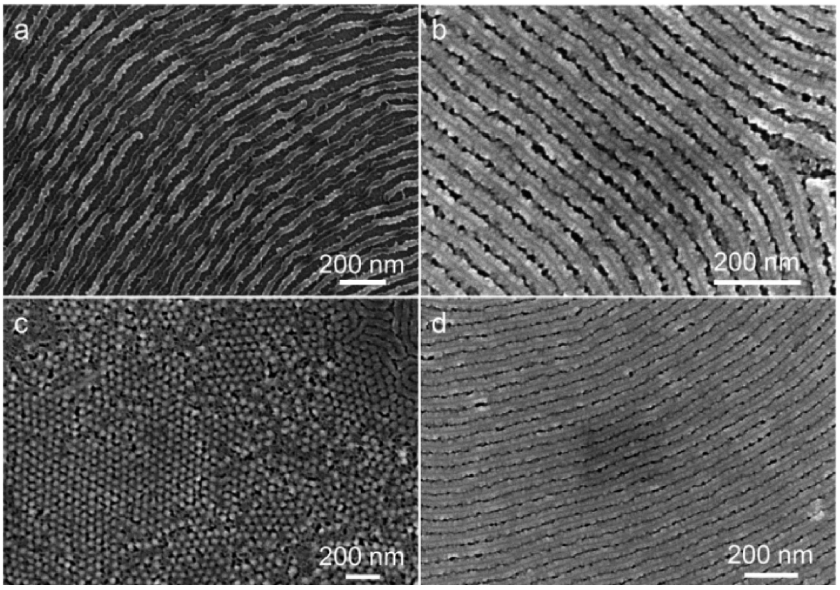

Figure 5. FESEM images of nanopatterns formed on Si wafer templated by a PS-*b*-PMMA thin film using: (a) 1 cycle of Al_2O_3 SIS followed by 10 cycles of W SIS. (b, c) 1 cycle of Al_2O_3 SIS followed by 20 cycles of W SIS, (d) 2 cycles of Al_2O_3 SIS followed by 20 cycles of W SIS. PS-*b*-PMMA was removed by O_2 plasma.

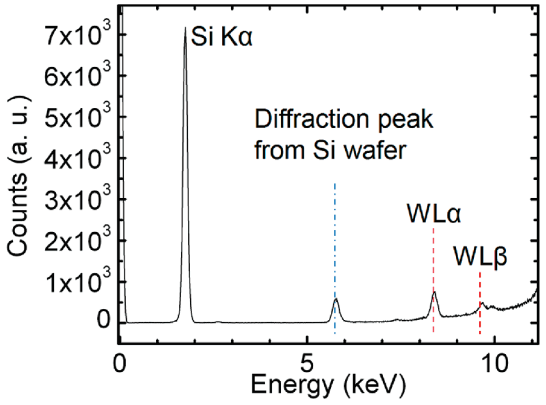

Figure 6. (a) X-ray fluorescence spectrum of PS-*b*-PMMA sample with 1 cycle Al_2O_3 SIS and 20 cycles W SIS before O_2 plasma treatment. The Al peak is not detectible due to overlap with the strong Si peak from the substrate.

PS-*b*-PMMA film. Moreover, as shown in Figure 5c, dense nanoposts with diameters of 40.3 ± 3.1 nm were also observed on the sample shown in Figure 5b, which again confirms the process can be extended to template different structures in BCPs.

XPS analysis was performed on the PS-*b*-PMMA sample treated with 2 cycles Al_2O_3 and 20 cycles W before removing the polymer. Figure 7a shows an XPS spectrum of the sample before sputter cleaning where the atomic concentrations for O, C, Si, and W are 36, 52, 8, and 4 atom %, while Al is not detected. After sputter cleaning for 8 min with a 5 KeV Ar^+ beam, XPS analysis shows that the W concentration has increased to ~20 atom % and Al becomes visible at ~10 atom %. XPS confirms the preferential deposition of W on the top surface of PMMA as well as the nonuniform W distribution suggested by SEM (Figure 5).

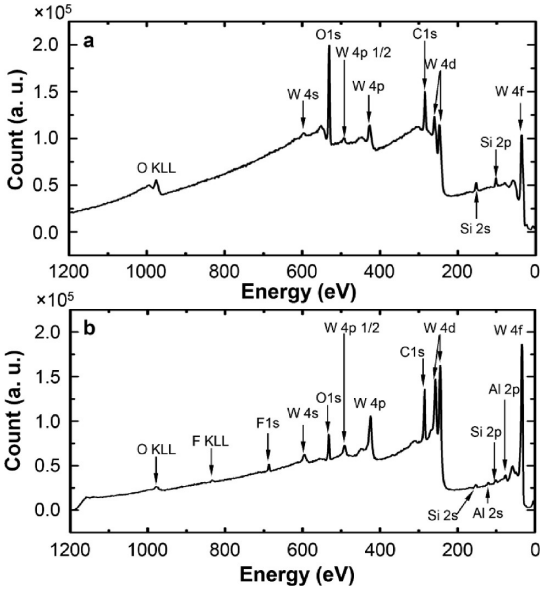

Figure 7. XPS spectra of self-assembled PS-*b*-PMMA coated Si wafer after 2 cycles of Al_2O_3 treatment followed by 20 cycles W SIS before removing the polymer. (a) Without Ar sputtering. O, C, Si, and W atomic concentrations are 36, 52, 8, and 4 atom %. (b) After Ar ion (5KeV) sputtering for 8 min. O, C, F, Si, Al, and W atomic concentrations are 9, 56, 1, 4, 10, and 20 atom % respectively. C is from polymer and adventitious contamination. Si and F are ascribed to impurities from the W deposition process.

CONCLUSIONS

The selective and controlled interaction between TMA and carbonyl groups in the PMMA domains of self-assembled block copolymer PS-*b*-PMMA substrates provides a new way to chemically modify the PMMA without disturbing the BCP assembly process. The localized Al−OH/Al−CH_3 sites formed in the

PMMA domains enable the SIS of nanoscopic materials such as SiO_2, ZnO, and W. This method could potentially be extended further to synthesize patterned designer materials with controlled size, spacing, symmetry, and composition through the rational design of BCPs and selection of SIS parameters.

EXPERIMENTAL SECTION

Materials. Sequential infiltration synthesis reactants including trimethyl aluminum ($Al(CH_3)_3$, TMA 96%), tri(tert-pentoxy) silanol (TPS, 99.99% trace metals basis), tungsten hexafluoride (WF_6, >99.9%) and disilane (Si_2H_6, 99.998%), were purchased from Sigma-Aldrich. Diethyl zinc (DEZ, >95%) was acquired from Strem. All chemicals listed above were used as received. Deionized H_2O was generated from an on-site purifier. Ultrahigh-purity N_2 (99.999%) was used as the purge gas and carrier gas with further purification by an inert gas filter (Aeronex Gatekeeper) before entering the reactor. PS-*b*-PMMA (M_W = 50500/20900) was purchased from Polymer Source, Inc. and purified through Soxhlet extraction to remove excess PS homopolymer. BCP solutions were prepared in toluene (Fisher, 99.5%) with a concentration of 13 mg/mL.

Block Copolymer Self-Assembly. PS_{485}-*b*-$PMMA_{201}$ block copolymer films were prepared by spin coating from a toluene solution onto cleaned silicon substrates with native SiO_2. After deposition, the PS-*b*-PMMA films were annealed at 250 °C for 2 h in a tube furnace under a flowing Ar atmosphere, then cooled down to room temperature in order to obtain self-assembled patterns. The in-plane PMMA cylinders were 30 ± 3 nm in diameter, and the center-to-center lateral distance was 60 ± 5 nm as shown before.[16]

Sequential Infiltration Synthesis. SIS was performed in a custom viscous flow ALD reactor as described previously.[33] Al_2O_3, SiO_2, ZnO, and tungsten (W) SIS were performed using binary reactions of TMA/H_2O,[17] TMA/TPS,[28,29] DEZ/H_2O,[30,31] and WF_6/Si_2H_6,[32] respectively within polymer substrates. The TPS was held in a stainless steel bottle, heated to 100 °C, that led directly into the reactor. All other precursors were introduced into the reactor as room temperature vapors. Si substrates with block copolymer coatings were loaded into the reactor on a stainless steel tray. To remove moisture and achieve thermal equilibrium, the samples were subjected to a 300 sccm N_2 flow at 1 Torr for at least 30 min and then evacuated to less than 20 mTorr before commencing SIS. The Al_2O_3, W, and ZnO SIS was performed in semistatic mode[34] as described in a previous work.[16] The experiment details of SIS in semistatic mode[16,34] is shown as follows: before the first reactant exposure, the chamber was first evacuated to ~20 mTorr. Next, 5 Torr of the first precursor was admitted into the reactor. After a predetermined exposure period, the excess reactants and byproducts were evacuated until reaching a pressure below 20 mTorr. The chamber was then purged with N_2 gas using a flow rate of 300 sccm at 1 Torr for a predetermined period. The chamber was then evacuated again below 20 mTorr. A similar evacuate−fill−purge−evacuate process was used for the second precursor reactant, and this entire sequence was repeated cyclically as in conventional ALD. The SIS timing sequence is given as a/b/c/d where a and c are the exposure times to the metal precursor and the coreactant, respectively, and c and d are the corresponding purge times with all times given in seconds (s). To verify that the SIS growth is not affected by unintended gas phase reactions, a bare Si substrate with native oxide (cleaned by sonicating in acetone, flushing with isopropyl alcohol, and drying with nitrogen gas) was used as a witness substrate for each run. Catalytic SiO_2 SIS was performed at 125 °C with 120 sccm N_2 flow at 0.55 Torr in continuous flow mode.[28,29] The timing for the TMA/purge/TPS/purge sequence was 400/1200/400/1200 s. The partial pressures for TMA and TPA during the precursor exposures were ~50 mTorr and 25 mTorr, respectively.

Characterization. Following SIS, the polymer component of the film was removed either by O_2 plasma etching or by heating in air at 400 °C for 12 h. O_2 plasma etching was performed at 50 W for 1 min in a March CS-1701 plasma etcher. A field emission scanning electron microscope (FESEM, Hitachi S-4700-II) was used to examine the surface of the resulting materials after polymer removal. The feature sizes were measured from the SEM images, and the mean values and corresponding standard deviations reported resulted from more than 50 measurements performed at different locations on the images. The SEM was equipped with an energy-dispersive X-ray (EDX) detector for elemental analysis. Spectroscopic ellipsometry (J. A. Woollam Co. Inc., alpha-SE) was used to evaluate the film thickness on the silicon witness samples. X-ray fluorescence (XRF) analysis was carried out on an Oxford Instruments ED2000. X-ray photoelectron spectroscopy (XPS) was performed with a Kratos Analytical Axis Ultra instrument with a monochromatic Al Kα (1486.6 eV) X-ray source operated at 15 kV. The C1s peak was normalized to 284.6 eV as the reference and 160 eV pass energy was used for the scan.

Acknowledgment. Use of the Center for Nanoscale Materials was supported by the U.S. Department of Energy, Office of Science, Office of Basic Energy Sciences, under Contract No. DE-AC02-06CH11357. This work was supported in part by the Argonne-Northwestern Solar Energy Research Center, an Energy Frontier Research Center funded by the U.S. Department of Energy, Office of Science, and Office of Basic Energy Sciences under Award Number DE-SC0001785.

Supporting Information Available: SEM image of the self-assembled PS-*b*-PMMA coated Si wafer after 10 cycles W SIS without TMA pretreatment followed by O_2 plasma treatment. This material is available free of charge *via* the Internet at http://pubs.acs.org.

REFERENCES AND NOTES

1. Whitesides, G. M.; Ostuni, E.; Takayama, S.; Jiang, X. Y.; Ingber, D. E. Soft Lithography in Biology and Biochemistry. *Annu. Rev. Biomed. Eng.* **2001**, *3*, 335–373.
2. Darling, S. B. Block Copolymers for Photovoltaics. *Energy Environ. Sci.* **2009**, *2*, 1266–1273.
3. Fasolka, M. J.; Mayes, A. M. Block Copolymer Thin Films: Physics and Applications. *Annu. Rev. Mater. Res.* **2001**, *31*, 323–355.
4. Bang, J.; Jeong, U.; Ryu, D. Y.; Russell, T. P.; Hawker, C. J. Block Copolymer Nanolithography: Translation of Molecular Level Control to Nanoscale Patterns. *Adv. Mater.* **2009**, *21*, 4769–4792.
5. Darling, S. B. Directing the Self-Assembly of Block Copolymers. *Prog. Polym. Sci.* **2007**, *32*, 1152–1204.
6. Kim, H. C.; Park, S. M.; Hinsberg, W. D. Block Copolymer Based Nanostructures: Materials, Processes, and Applications to Electronics. *Chem. Rev.* **2010**, *110*, 146–177.
7. Chen, D.; Park, S.; Chen, J. T.; Redston, E.; Russell, T. P. A Simple Route for the Preparation of Mesoporous Nanostructures Using Block Copolymers. *ACS Nano* **2009**, *3*, 2827–2833.
8. Jeong, S. J.; Xia, G. D.; Kim, B. H.; Shin, D. O.; Kwon, S. H.; Kang, S. W.; Kim, S. O. Universal Block Copolymer Lithography for Metals, Semiconductors, Ceramics, and Polymers. *Adv. Mater.* **2008**, *20*, 1898–1904.
9. Kim, H. C.; Jia, X. Q.; Stafford, C. M.; Kim, D. H.; McCarthy, T. J.; Tuominen, M.; Hawker, C. J.; Russell, T. P. A Route to Nanoscopic SiO_2 Posts *via* Block Copolymer Templates. *Adv. Mater.* **2001**, *13*, 795–797.

10. Park, S.; Kim, B.; Wang, J. Y.; Russell, T. P. Fabrication of Highly Ordered Silicon Oxide Dots and Stripes from Block Copolymer Thin Films. *Adv. Mater.* **2008**, *20*, 681–685.
11. van Zoelen, W.; Vlooswijk, A. H. G.; Ferri, A.; Andringa, A. M.; Noheda, B.; ten Brinke, G. Ordered Arrays of Ferroelectric Nanoparticles by Pulsed Laser Deposition on PS-*b*-P4VP-(PDP) Supramolecule-Based Templates. *Chem. Mater.* **2009**, *21*, 4719–4723.
12. Kim, D. H.; Kim, S. H.; Lavery, K.; Russell, T. P. Inorganic Nanodots from Thin Films of Block Copolymers. *Nano Lett.* **2004**, *4*, 1841–1844.
13. Lopes, W. A.; Jaeger, H. M. Hierarchical Self-Assembly of Metal Nanostructures on Diblock Copolymer Scaffolds. *Nature* **2001**, *414*, 735–738.
14. Cheng, J. Y.; Mayes, A. M.; Ross, C. A. Nanostructure Engineering by Templated Self-Assembly of Block Copolymers. *Nat. Mater.* **2004**, *3*, 823–828.
15. Jinan, C.; Dong, W.; Xiangning, F.; Buriak, J. M. Assembly of Aligned Linear Metallic Patterns on Silicon. *Nat. Nanotechnol.* **2007**, *2*, 500–506.
16. Peng, Q.; Tseng, Y.-C.; Darling, S. B.; Elam, J. W. Nanoscopic Patterned Materials with Tunable Dimensions *via* Atomic Layer Deposition on Block Copolymers. *Adv. Mater.* **2010**, *22*, 5129–5133.
17. Peng, Q.; Sun, X. Y.; Spagnola, J. C.; Hyde, G. K.; Spontak, R. J.; Parsons, G. N. Atomic Layer Deposition on Electrospun Polymer Fibers as a Direct Route to Al_2O_3 Microtubes with Precise Wall Thickness Control. *Nano Lett.* **2007**, *7*, 719–722.
18. George, S. M. Atomic Layer Deposition: An Overview. *Chem. Rev.* **2010**, *110*, 111–131.
19. Leskela, M.; Ritala, M. Atomic Layer Deposition Chemistry: Recent Developments and Future Challenges. *Angew. Chem., Int. Ed.* **2003**, *42*, 5548–5554.
20. Wang, Y.; Qin, Y.; Berger, A.; Yau, E.; He, C. C.; Zhang, L. B.; Gosele, U.; Knez, M.; Steinhart, M. Nanoscopic Morphologies in Block Copolymer Nanorods as Templates for Atomic Layer Deposition of Semiconductors. *Adv. Mater.* **2009**, *21*, 2763–2766.
21. Ras, R. H. A.; Kemell, M.; de Wit, J.; Ritala, M.; ten Brinke, G.; Leskela, M.; Ikkala, O. Hollow Inorganic Nanospheres and Nanotubes with Tunable Wall Thicknesses by Atomic Layer Deposition on Self-Assembled Polymeric Templates. *Adv. Mater.* **2007**, *19*, 102–105.
22. Sinha, A.; Hess, D. W.; Henderson, C. L. Area Selective Atomic Layer Deposition of Titanium Dioxide: Effect of Precursor Chemistry. *J. Vac. Sci. Technol. B* **2006**, *24*, 2523–2532.
23. Sinha, A.; Hess, D. W.; Henderson, C. L. Transport Behavior of Atomic Layer Deposition Precursors through Polymer Masking Layers: Influence on Area Selective Atomic Layer Deposition. *J. Vac. Sci. Technol. B* **2007**, *25*, 1721–1728.
24. Lee, S. M.; Pippel, E.; Gosele, U.; Dresbach, C.; Qin, Y.; Chandran, C. V.; Brauniger, T.; Hause, G.; Knez, M. Greatly Increased Toughness of Infiltrated Spider Silk. *Science* **2009**, *324*, 488–492.
25. Zhang, L. B.; Patil, A. J.; Li, L.; Schierhorn, A.; Mann, S.; Gosele, U.; Knez, M. Chemical Infiltration during Atomic Layer Deposition: Metalation of Porphyrins as Model Substrates. *Angew. Chem., Int. Ed.* **2009**, *48*, 4982–4985.
26. Puurunen, R. L. Surface Chemistry of Atomic Layer Deposition: A Case Study for the Trimethylaluminum/Water Process. *J. Appl. Phys.* 2005, *97*, 121301, 1-52.
27. George, S. M.; Ott, A. W.; Klaus, J. W. Surface Chemistry for Atomic Layer Growth. *J. Phys. Chem.* **1996**, *100*, 13121–13131.
28. Burton, B. B.; Boleslawski, M. P.; Desombre, A. T.; George, S. M. Rapid SiO_2 Atomic Layer Deposition Using Tris(tert-pentoxy)silanol. *Chem. Mater.* **2008**, *20*, 7031–7043.
29. Hausmann, D.; Becker, J.; Wang, S. L.; Gordon, R. G. Rapid Vapor Deposition of Highly Conformal Silica Nanolaminates. *Science* **2002**, *298*, 402–406.
30. Yousfi, E. B.; Fouache, J.; Lincot, D. Study of Atomic Layer Epitaxy of Zinc Oxide by *in-Situ* Quartz Crystal Microgravimetry. *Appl. Surf. Sci.* **2000**, *153*, 223–234.
31. Peng, Q.; Sun, X. Y.; Spagnola, J. C.; Saquing, C.; Khan, S. A.; Spontak, R. J.; Parsons, G. N. Bi-directional Kirkendall Effect in Coaxial Microtuble Nanolaminate Assemblies Fabricated by Atomic Layer Deposition. *Acs Nano* **2009**, *3*, 546–554.
32. Wilson, C. A.; McCormick, J. A.; Cavanagh, A. S.; Goldstein, D. N.; Weimer, A. W.; George, S. M. Tungsten Atomic Layer Deposition on Polymers. *Thin Solid Films* **2008**, *516*, 6175–6185.
33. Elam, J. W.; Groner, M. D.; George, S. M. Viscous Flow Reactor with Quartz Crystal Microbalance for Thin Film Growth by Atomic Layer Deposition. *Rev. Sci. Instrum.* **2002**, *73*, 2981–2987.
34. Kemell, M.; Ritala, M.; Leskela, M.; Groenen, R.; Lindfors, S. Coating of Highly Porous Fiber Matrices by Atomic Layer Deposition. *Chem. Vap. Deposition* **2008**, *14*, 347–352.